Research Article | Vol. 27, No. 3 | 4 Feb 2019 | OPTICS EXPRESS 2374
Optics EXPRESS

Gouy phase effects on propagation of pure and hybrid vector beams

María M. Sánchez-López,[1,*] Jeffrey A. Davis,[2] Ignacio Moreno,[3] Aarón Cofré,[3] and Don M. Cottrell[2]

[1]*Instituto de Bioingeniería. Departamento de Física y Aplicada. Universidad Miguel Hernández de Elche. 03202 Elche, Spain*
[2]*Department of Physics. San Diego State University, San Diego, California 92182-1233, USA*
[3]*Departamento de Ciencia de Materiales, Óptica y Tecnología Electrónica. Universidad Miguel Hernández de Elche. 03202 Elche, Spain*
[*]*mar.sanchez@umh.es*

Abstract: The robustness of the polarization spatial distribution of vector beams upon propagation is crucial for a number of applications, including optical communications and materials processing. This study has been commonly centered on Gouy phase effects on focused vector beams. In this work, we present a theoretical and experimental analysis of the Gouy phase's effects on the propagation of pure and hybrid vector beams. Experimental results at various axial planes, before and past the focus, are obtained by using a simplified liquid-crystal spatial light modulator-based optical system that allows the easy generation of these beams. Furthermore, a new alternative optical set-up that is devoid of moving elements is demonstrated, which simplifies this study. We experimentally verify the differences between pure and hybrid vector beams upon propagation. While the first ones remain stable, hybrid vector beams show Gouy phase effects that demonstrate an optical activity where the local polarization states rotate by an angle that depends on the propagation distance. Experimental results agree with the theory.

1. Introduction

Vector beams are of interest for their polarization spatial distribution and they received a great deal of attention for their applications in many diverse fields [1]. Particular interest is their use to optically encode and transmit information either via free space [2] or through optical fibers [3]. The stability of the polarization structure of vector beams as they propagate is very relevant for such applications. In addition, other groups are examining their use for material processing where focused vector beams are employed to imprint subwavelength patterns [4]. It is known that pure vector beams retain their polarization pattern. But related variants like hybrid or truncated vector beams experience significant deformation upon propagation.

Pure vector beams are the superposition of right (RCP) and left (LCP) circularly polarized components with helical phases having opposite topological charges $\ell_R = -\ell_L$ [5]. Initially they were generated interferometrically [6], but nowadays it is common to use devices named *q*-plates [7]. These are half-wave retarders where the orientation of the axis rotates azimuthally proportional to the *q*-value. These geometric phase devices introduce helical phases with charges $\pm 2q$ onto the RCP and LCP states. Alternatively, pure vector beams can be generated using programmable spatial light modulators (SLMs) where spiral phase plates (SPPs) with opposite charges $\ell_R = -\ell_L = \ell$ are encoded onto the two orthogonal polarizations, thus mimicking an equivalent *q*-plate device with a *q*-value $q = \ell/2$ [7]. Different optical setups with different SLM configurations have been proposed to generate vector beams [8–10]. While bulkier, these SLM-based systems have a great deal of flexibility

#351955 https://doi.org/10.1364/OE.27.002374
Journal © 2019 Received 15 Nov 2018; revised 21 Dec 2018; accepted 31 Dec 2018; published 25 Jan 2019

Optics EXPRESS

to examine new ideas before adding the expense of fabricating their physical *q*-plate counterparts.

Hybrid vector beams are variations where SPPs with different topological charges ℓ_R and ℓ_L are encoded onto the orthogonal polarization components. They received different names such as pseudo-vortex beams [11], Poincaré beams [12], vectorial vortices [13], vector vortex beams [14], or cylindrically polarized beams of the hybrid Poincaré sphere [15]. A first very simple approach to generate hybrid vector beams is a radial polarizer illuminated with circularly polarized light [11]. The output is radially polarized, but the decomposition of the circular polarization components reveal that they have charges $\ell_R = 0$ and $\ell_L = 0$. The same situation occurs when a single SLM is used in between QWPs to generate a polarization azimuthal rotator, since only one polarization component can be modulated [16]. In these cases, one polarization component has zero charge and the entire topological charge is encoded in the orthogonal polarization component. These beams can be identified as Poincaré beams [12]. Other approaches to generate hybrid vector beams involve forked gratings [15], a *q*-plate and a spiral phase plate (SPP) [13,14], an equivalent *q*-plate system and a single SLM [17], or a *q*-plate operating at quarter-wave retardance [18]. In all cases the topological charges encoded onto orthogonal polarizations follow $\ell_R \neq -\ell_L$. Again, the use of SLM based systems allows the independent manipulation of the topological charges to generate arbitrary hybrid vector beams [19,20].

Under certain circumstances, the polarization patterns are similar for pure and hybrid vector beams. However, their propagation dynamics are very different, affected by the different Gouy phase that the two orthogonal polarization components experience for different topological charges [21–23]. Such Gouy effects have been compared for pure vector and non-pure vector beams [24], showing that pure vector beams retain their polarization pattern. Rotating optical fields have been previously described, for instance by the combination of scalar Bessel-Gauss beams with different phase velocities [25]. More recently, the Gouy phase has been identified as responsible of the rotation observed in partially truncated scalar vortex beams [26–28]. Recent studies also manifested that truncated vector beams experience significant deformation of its structure upon propagation caused by the Gouy phase [29,30].

Therefore, it is of great interest to develop optical arrangements where the propagation dynamics of different vector beams can be easily studied and compared. This work presents a simplified optical system that enables the systematic study of Gouy phase effects on vector beams. First, using only one liquid-crystal SLM and one *q*-plate device, similarly to [17], we readily generate pure and hybrid vector beams. These beams are examined on the basis of the Gouy phase shift difference experienced by the RCP and LCP components, depending on the charge encoded in each component. An equivalent optical activity phenomena upon propagation caused by the Gouy phase is demonstrated, that explains the polarization transformations observed between the generated near field and the propagated far field pattern. This study is performed by analyzing the axial propagation. Second, we demonstrate that the same experimental analysis can be performed without any moving element by applying a virtual propagation procedure [31,32] based on the application of a fast Fresnel diffraction algorithm [33], thus simplifying the experimental load of this type of study.

2. Gouy phase in pure and hybrid vector beams

We follow [34] for the definition of the Gouy phase, and concentrate on Laguerre-Gauss modes $LG_{p\ell}$ where p is the radial index and ℓ is the azimuthal index. For simplicity, we only consider the vortex modes $LG_{0\ell}$ having spiral phase of charge ℓ and radial index $p = 0$. These modes can be characterized by an electric field as

Optics EXPRESS

$$E_\ell = u_{0\ell}(z)e^{-i\ell\theta}e^{-i\Phi(\ell,z)}, \tag{1}$$

where $u_{0\ell}(z)$ is a complex amplitude term given by [34,35]:

$$u_{0\ell}(z) = \sqrt{\frac{1}{\pi(|\ell|)!}}\frac{1}{\omega(z)}\left(\frac{\sqrt{2}r}{\omega(z)}\right)^{|\ell|} L_0^{|\ell|}\left(\frac{2r^2}{\omega(z)^2}\right)\exp\left(\frac{-r^2}{\omega(z)^2} - i\frac{kr^2}{2R(z)}\right), \tag{2}$$

where $R(z)$ and $\omega(z)$ are the radius of curvature and beam width respectively. We note that these $LG_{0\ell}$ modes are usually identified as optical vortex beams whose diameter depends not only on the waist size, but also on the charge ℓ of the spiral phase [36].

The Gouy phase $\Phi(p,\ell,z)$ for a $LG_{p\ell}$ mode is given by

$$\Phi(p,\ell,z) = [|\ell|+2p+1]\zeta(z), \tag{3}$$

where $\zeta(z) = \tan^{-1}(z/z_0)$. Here $z_0 = \pi\omega_0^2/\lambda$ and ω_0 are the Rayleigh range and the beam width at the waist, respectively. Figure 1 shows $\zeta(z)$ as a function of propagation distance z around the beam waist, which is located at $z=0$. It reaches limits of $\pm\pi/2$ at distances of $z=\pm\infty$, but values of $\pm\pi/4$ at distances of only $z=\pm z_0$. However, these variations of the Gouy phase are magnified by the parameter $|\ell|+2p+1$ in Eq. (3), which depends on the absolute value of ℓ. This has important physical implications, as shown later.

For the zero order Gaussian beam, the beam width $\omega(z)$ increases with propagation distance in both directions away from the waist as

$$\omega(z) = \omega_0\sqrt{1+\left(\frac{z}{z_0}\right)^2}. \tag{4}$$

Therefore, for narrower beam waist ω_0 the Rayleigh range z_0 is smaller, and consequently the beam will expand more quickly.

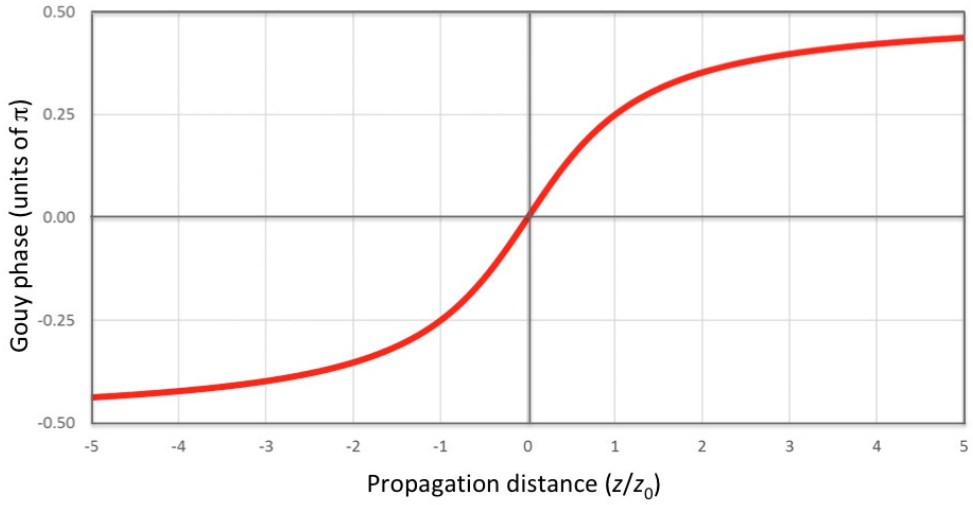

Fig. 1. Plot of the Gouy phase term $\zeta(z)$ in Eq. (1).

Optics EXPRESS

The situation is more complicated for the LG modes because the beam width depends on both the Gaussian beam width ω_0 and the charge ℓ. The divergence of LG modes has been recently discussed [37,38]. For our considerations, there is not a simple relationship to determine the value of z_0 and we will rely on computer simulations. For this work, we will arbitrarily define an "effective" z_0 as the distance for the Gouy phase term $\zeta(z)$ to change by $\pi/4$ in Fig. 1. For the case of a Gaussian beam $(\ell = 0)$, this coincides with the standard definition of the Rayleigh range.

A vector beam can be regarded as the superposition of two $LG_{0\ell}$ beams in Eq. (1) encoded onto the RCP and LCP states and with different charges ℓ_R and ℓ_L. For simplification, we only consider the case of linearly polarized vector beams, thus both circular polarization components have the same weight. Then, the vector beam can be written as:

$$\left|V(z)\right\rangle = u_{0\ell_R}(z)e^{-i\ell_R\theta}e^{-i\Phi_R(\ell,z)}\left|R\right\rangle + u_{0\ell_L}(z)e^{-i\ell_L\theta}e^{-i\Phi_L(\ell,z)}\left|L\right\rangle, \tag{5}$$

where $\left|R\right\rangle = \frac{1}{\sqrt{2}}(1,+i)^t$ and $\left|L\right\rangle = \frac{1}{\sqrt{2}}(1,-i)^t$ denote the normalized Jones vectors for the RCP and LCP states. Here the Gouy phase for the RCP and LCP components are

$$\Phi_R(z) = \left[|\ell_R|+1\right]\zeta(z) \text{ and } \Phi_L(z) = \left[|\ell_L|+1\right]\zeta(z). \tag{6}$$

Thus, when $|\ell_R| = |\ell_L|$ the Gouy phase is the same for the RCP and LCP components. However, when $|\ell_R| \neq |\ell_L|$ there is a phase shift between these polarization components as the beam propagates.

It is well known that a phase shift between the circular polarization components is the cause of the optical activity, i.e. a rotation of the state of polarization [39,40]. In this case, the phase difference depends on the propagation distance, and therefore this effect can be regarded as an axially dependent optical activity. Also note that the sense of the optical activity depends on the difference $|\ell_R| - |\ell_L|$, so the polarization transformation upon propagation can be levorotatory or dextrorotatory (similar to the difference between sugar and fructose) [40]. Therefore, a rotation of the polarization pattern is expected due to the Gouy phase difference $\Delta\Phi_G(z)$ between the RCP and LCP components, which depends on the encoded charges as

$$\Delta\Phi_G(z) = \Phi_R(z) - \Phi_L(z) = \left(|\ell_R| - |\ell_L|\right)\zeta(z). \tag{7}$$

In order to calculate the rotation angle of the polarization, it is useful to define the mean topological charge (ℓ) and the semi-subtraction of the topological charges (m) as:

$$\ell = \tfrac{1}{2}(\ell_R + \ell_L) \text{ and } m = \tfrac{1}{2}(\ell_R - \ell_L). \tag{8}$$

Note that pure vector beams have $\ell = 0$, while $\ell \neq 0$ for hybrid vector beams. Note also, that in the case of hybrid vector beams, the RCP and LCP vortex components are of different diameter [37,38], i.e., the complex amplitudes $u_{0\ell_R}$ and $u_{0\ell_L}$ in Eq. (5) are different.

For simplicity, let us approximate $u_{0\ell_R}(z) \approx u_{0\ell_L}(z) \approx u_{0\ell}(z)$. We discuss the limitations of this approximation below and in the conclusions. Then, using these ℓ and m parameters, Eq. (5) can be approximated as

$$\left|V(z)\right\rangle \simeq u_{0\ell}e^{-i\ell\theta}\left\{e^{-im\theta}e^{-i\Phi_R(z)}\left|R\right\rangle + e^{+im\theta}e^{-i\Phi_L(z)}\left|L\right\rangle\right\}, \tag{9}$$

and the polarization rotation is given by:

Optics EXPRESS

$$\alpha(z) = \tfrac{1}{2}\Delta\Phi_G(z) = \tfrac{1}{2}\left(|\ell + m| - |\ell - m|\right)\zeta(z). \tag{10}$$

Note that this last equation was reported in [24], where in that case ℓ and m were the topological charge produced by a fork-grating and an encoded q-plate, respectively.

Here, it is important to emphasize that this analysis is only an approximation useful to get a physical insight on how the polarization pattern of hybrid vector beams rotates as the beam propagates. Because of the size difference between $LG_{0\ell}$ modes having different angular phases, it cannot account for a precise quantitative description of the rotation angle. As a result, the distribution of polarization states and intensity will not only rotate but also change structure as a whole. However, the simplicity of the above analysis is very valuable to obtain an approximated insight of the polarization transformation upon propagation, with still quite good accurate description, as will be further discussed in the next section.

Finally, within this approximation, and following the definitions of $|R\rangle$ and $|L\rangle$, Eq. (9) can be written as the following Jones vector:

$$|V(z)\rangle = 2u_{0\ell}e^{-i\ell\theta}e^{-i\frac{1}{2}(\Phi_R(z)+\Phi_L(z))}\begin{pmatrix}\cos\left(m\theta+\alpha(z)\right)\\ \sin\left(m\theta+\alpha(z)\right)\end{pmatrix}. \tag{11}$$

Note that Eq. (11) corresponds to a linear vector beam, where the rotation angle $\alpha(z)$ defined in Eq. (10) implies a change of origin of the vector beam polarization state. For instance, for the vector beam of order $m=1$, the radial, slanted, azimuthal and opposite slanted vector beams are obtained for $\alpha(z) = 0, \pi/4, \pi/2$ and $3\pi/4$.

For a pure vector beam $\ell_R = -\ell_L$ and $\ell = 0$. Therefore, according to Eqs. (10) and (11), the Gouy phase shift difference is zero and the optical rotation is null. Thus, the Gouy phase does not have any impact on the propagation of pure vector beams. However, different pairs of charges (ℓ_R, ℓ_L) can correspond to the same value of m (and therefore to the same initial spatial distribution of polarization states) but with $\ell \neq 0$. This implies a non-null polarization rotation $\alpha(z)$ as the beam propagates, that has a great importance in the propagation dynamics. In [23] Zhang *et al* studied these effects when $\ell_R \neq -\ell_L$. However, their experimental study was limited only to the beam focused at the focus of a converging lens. But let us point out that the verification of the polarization rotation as the beam propagates requires measurements at distances of approximately z_0 from the waist of the Gaussian beam.

As mentioned earlier, because of the size difference between $LG_{0\ell}$ modes having different angular phases, there is a limit on whether these beams will overlap if the value of m is too large, and the above approximation $u_{0\ell_R}(z) \approx u_{0\ell_L}(z) \approx u_{0\ell}(z)$ can be applied. Nevertheless, as we show next, this approximation provides a qualitative good description if m is kept small.

3. Experimental procedure

We first note here that experimental studies of these effects depend strongly on the size of the beam waist. For example, consider a beam having a beam waist of $\omega_0 = 4$ mm, which is a typical size for vector beams generated by SLM-based optical set-ups. For our laser source of 632.8 nm, the value of z_0 is 80 meters and cannot be realized in the laboratory.

Instead it is useful to use a lens to reduce the beam waist, as shown in Fig. 2. Here, a Gaussian beam having a beam waist ω_{01} is incident at its waist onto a lens having a focal length f and the new beam waist ω_{02} is formed approximately at the focal plane. This new beam waist is given [41] by

Optics EXPRESS

$$\omega_{02} \simeq \omega_{01} \frac{f}{z_{01}} \tag{12}$$

Therefore, the new Rayleigh range is reduced to

$$z_{02} \simeq \frac{f^2 \lambda}{\pi \omega_{01}^2} \tag{13}$$

where Eq. (12) and the definitions of the Rayleigh ranges z_{01} and z_{02} were used.

The system in Fig. 2 has two advantages. First, the size of the Rayleigh range is reduced to values compatible with the laboratory. In addition, this setup allows us to study the Gouy phase on either side of the beam waist. An SLM and a *q*-plate located before the lens are used to generate different kinds of vector beams. Pure vector beams are obtained by turning the SLM off and using only the *q*-plate, while hybrid vector beams require both the *q*-plate and the SLM with the desired spiral phase encoded.

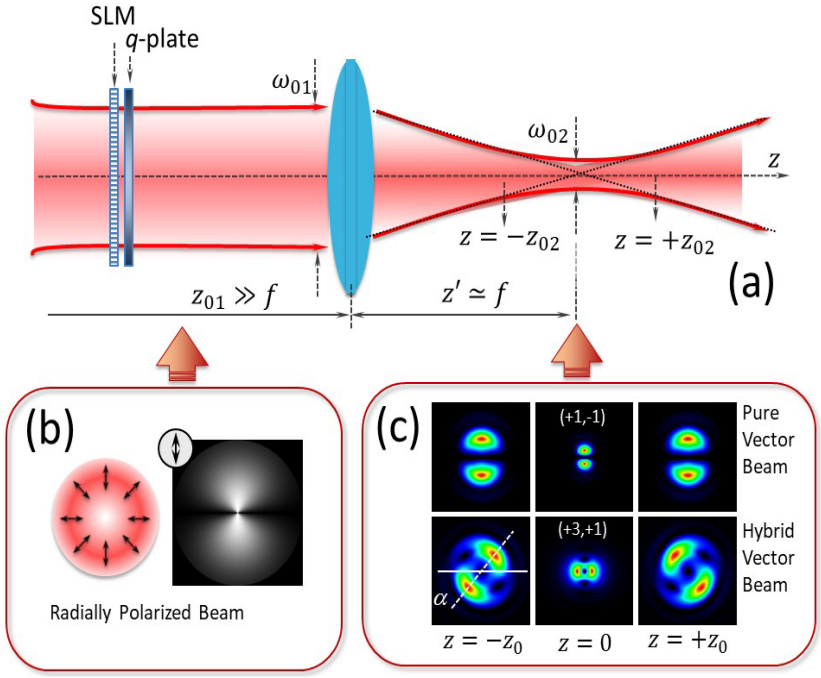

Fig. 2. (a) Focusing of a Gaussian beam with a lens. The new smaller waist is located approximately at the focal plane of the lens. The waist is located at the position $z = 0$. An SLM and a q-plate located before the lens are used to generate the vector beam. Simulation results in (b) and (c) for the intensity pattern behind an analyzer that is vertically aligned and at various axial locations. (b) Right after the SLM and *q*-plate, pure and hybrid vector beams show identical patterns. (c) However, when viewed around the focal plane the pure vector beam retains its polarization structure, while the hybrid vector beam suffers a rotation $\alpha(z)$.

The inset in Fig. 2 illustrates the situation for a radially polarized beam with two possible combinations of charges, $(\ell_R, \ell_L) = (+1, -1)$ and (+3, +1). They both yield the radially polarized beam of m = 1. However, the first combination corresponds to the pure radial polarization, while the second case is a hybrid version of this vector beam. If the beam is analyzed with a vertically oriented analyzer, the intensity pattern right after the SLM/*q*-plate system (inset b) shows in both cases two bright lobes oriented vertically and a dark line in the horizontal direction. However, when the beam is analyzed around the lens focus (inset c), the

Optics EXPRESS

behavior is quite different. While the two-lobe pattern is maintained for the pure vector beam, the hybrid vector beam rotates around the beam waist and achieves a 90° rotation at the focus. This rotation at the focus was already reported in [24]. However, here we explore in detail the rotation before and behind the focus.

These effects can be explained by the Gouy phase difference between the RCP and LCP components, as mentioned before. According to Eqs. (9)-(10), the polarization state rotates by an angle $\alpha(z)$. For the pure vector beam $(\ell = 0)$, Eq. (10) predicts $\alpha(z) = 0$ and therefore no rotation occurs. However, for the hybrid vector beam with $(\ell_R, \ell_L) = (+3, +1)$ Eq. (10) predicts a continuous polarization rotation $\alpha(z) = \zeta(z)$ which, therefore, follows the curve in Fig. 1. Note that the limit $z \to -\infty$, where $\alpha(z) = -\pi/2$, corresponds to the beam generated after the SLM/*q*-plate system. In this limit, the hybrid beam shows the two bright lobes oriented in the vertical direction. However, as it propagates, the polarization state rotates as $\alpha(z) = \zeta(z)$, and so does the intensity pattern transmitted by the vertical analyzer. At $z = -z_0$, the rotation is $\alpha(z) = -\pi/2$, while at the beam waist (z = 0) it is $\alpha(z) = 0$. Note that this means that the orientation of the two bright lobes becomes horizontal at the beam waist (Fig. 2(c)), i.e., the hybrid radially polarized vector beam is transformed at the focus into an azimuthal polarization. We note that this transformation from a radial polarization onto an azimuthal polarization was reported in Refs [24,42], but only at the focus plane and with a different setup. Past the waist, the beam continues rotating and it would show again the two bright lobes oriented along the vertical direction in the limit $z \to +\infty$, where $\alpha(z) = +\pi/2$.

These simulations show that the tendency is correctly described by the function $\zeta(z)$. However, it is important to note that the above analysis in terms of the rotation function $\alpha(z)$ is only a very useful simplification, since the approximation $u_{0\ell_R}(z) \approx u_{0\ell_L}(z)$ in Eq. (9) is considered. Vortex beams with topological charges 3 and 1 focalize in doughnut shapes, but with different diameters. Thus, their overlapping is not as perfect as it is in the case of the pure vector beam, and therefore the azimuthal polarization pattern is not perfect.

Nevertheless, as we show next, the axial optical activity caused by the Gouy phase difference provides a valid physical insight of the beam polarization pattern around the axis. In the next section, we discuss our experimental system and compare experimental results to computer simulations.

4. Experimental system and results

Figure 3(a) shows the experimental system we have developed to verify these effects. Light from a linearly polarized 20 mW He-Ne laser having a beam diameter of 0.7 mm at the $1/e^2$ points (so this is twice the value of ω_0) is spatially filtered using a X10 objective lens with a focal length of 14.8 mm and a 25 micron pinhole. The beam is then collimated using a 20 cm focal length lens (L1). The final width of the collimated beam is $\omega_0 \simeq 4$ mm. The beam then passes through a non-polarizing beam splitter (NPBS) and addresses the LCoS SLM.

The reflected beam impacts a reflective liquid-crystal on silicon (LCoS) spatial light modulator (SLM) manufactured by Hamamatsu (X10468 series), with 792 × 600 pixels having dimensions of $\Delta = 20$ μm. The phase shift is controlled over 2π radians at the He-Ne laser wavelength of 632.8 nm. The SLM liquid crystal director is oriented horizontally. Therefore, the input laser beam is selected to be linearly polarized along the horizontal direction so the SLM acts as a phase-only modulator. A spiral phase pattern (SPP) with charge ℓ_{SPP} is addressed onto the SLM. The beam then passes back through the NPBS and through a commercial *q*-plate from Thorlabs, identified as vortex half-wave retarder, with value q = 1/2.

Optics EXPRESS

As discussed in the introduction, the q-plate introduces a helical phase with charges ± $2q$ onto the RCP and LCP states. As a result, the RCP and LCP components now have charges $\ell_R = \ell_{2q} + \ell_{SPP}$ and $\ell_R = -\ell_{2q} + \ell_{SPP}$. The mean topological charge (ℓ) and the semi-subtraction of the topological charges (m) of the output vector beam are

$$\ell = \tfrac{1}{2}(\ell_R + \ell_L) = \ell_{SPP} \text{ and } m = \tfrac{1}{2}(\ell_R - \ell_L) = \ell_{2q}. \quad (14)$$

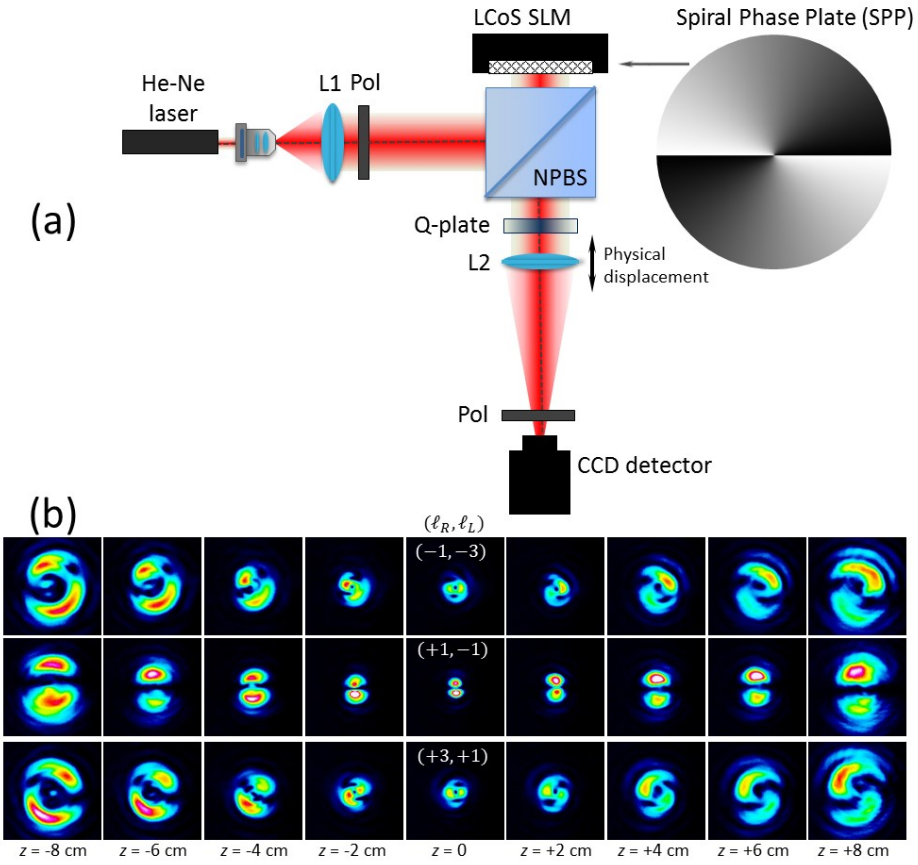

Fig. 3. (a) Scheme of the first proposed optical system to generate pure and hybrid vector beams and study the Gouy phase effects. A SPP is encoded on the LCoS-SLM and the lens L2 (or the CCD camera) is shifted longitudinally to capture different axial planes near the beam waist. (b) Experimental results for the propagation of the radially polarized beams with charges $(\ell_R, \ell_L) = (-1, -3)$, $(+1, -1)$ and $(+3, +1)$ The analyzer is vertically aligned in all cases.

For the case where no SPP is encoded onto the SLM, the q-plate creates a vector beam with $\ell_R = -\ell_L = 1$, thus with $\ell = 0$ and $m = 1$, i.e. a first order pure vector beam. However, when an SPP of charge ℓ_{SLM} is encoded on the SLM, the output is a hybrid vector beam with charges $\ell_R = \ell_{SLM} + 1$ and $\ell_R = \ell_{SLM} - 1$, thus with $\ell = \ell_{SLM}$, while keeping $m = 1$. Thus, the output is a first-order hybrid vector beam. Although the q-plate is fixed, the sign and value of $\ell = \ell_{SLM}$ encoded on the SPP can be controlled.

Finally, the transmitted light passes through a lens having a focal length of 100 cm (L2). The new smaller waist is formed at a detector whose axial position can be adjusted. Assuming a wavelength of $\lambda = 632.8$ nm and since $\omega_{01} = 4$ mm, Eqs. (12) and (13) provide the

Optics EXPRESS

expected values of $\omega_{02} \approx 50$ microns and $z_{02} \approx 12.6$ mm. A linear polarizer placed in front of the detector is used to analyze the pattern of the generated vector beam. The output is captured using a WinCamD CCD camera. The propagation characteristics of the generated pure and hybrid vector beams were studied by moving either the lens (L2) or the detector.

Figure 3(b) presents the experimental results for cases $(\ell_R, \ell_L) = (-1, -3)$, $(+1, -1)$ and (+3, +1). For these three cases, we first verified the generation of a radially polarized beam right after the *q*-plate and before lens L2. We verified this by placing an analyzer oriented vertically and noting the vertical orientation of the two bright lobes. Then, we analyzed the intensity pattern captured by the CCD detector around the focus of the focusing lens (L2). Different axial planes at distances z = 0, ±2, ±4, ±6, and ±8 cm, were captured by moving the focusing lens (L2). In each case, we show 456 × 456 pixels, where the size of the WinCam detector pixel is 4.65 microns. The experiments confirm the situation illustrated in Fig. 2.

As expected, the pure vector beam with charges $(\ell_R, \ell_L) = (+1, -1)$ (middle row) retains the two bright lobes in the vertical direction and a dark horizontal line. This verifies that the radial polarization is kept along the propagation. The only difference upon propagation is the different size of the beam, which reaches its smallest size at the focus.

This is not the case of the two hybrid vector beams with $(\ell_R, \ell_L) = (+3, +1)$ and $(-1, -3)$. They have the same semi-subtraction charge index m = +1 and therefore the beam is radially polarized behind the SLM-q-plate system. However, their propagation is quite different. Namely, the intensity pattern rotates as the beam approaches the focus, producing the characteristic "S" shaped beam caused by the lobes deformation. The sense of rotation is opposite in each case, as expected from Eq. (10). Note how at the focus the orientation of the lobes is rotated by 90° with respect to the pure radial polarization, denoting a 90° rotation in the state of polarization. However, at large distance from the focus in both directions, the lobes return to the vertical orientation. Finally, let us point out that the 45° polarization rotation occurs approximately at z = 40 mm, which is not the Rayleigh range of the Gaussian beam $z_{02} \approx 12.6$ mm mm that was calculated using Eq. (13). This value of 40 mm can then be regarded as an "effective" Rayleigh range for the hybrid vector beam.

Nevertheless, the arctan function $\zeta(z)$ in Fig. 1 describes qualitatively the rotation of the polarization state of these beams. The exact relation between the polarization rotation and the function $\zeta(z)$ depends on the encoded charges ℓ_R and ℓ_L, and on the input beam width.

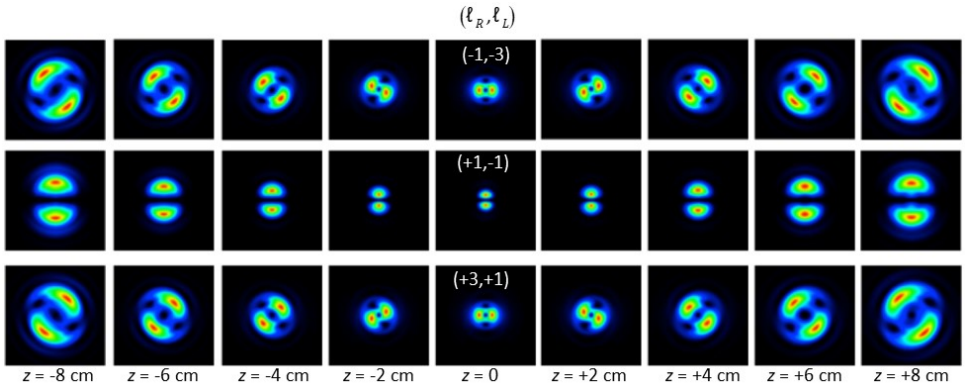

Fig. 4. Simulation results for the propagation of radially polarized beams with charges $(\ell_R, \ell_L) = (-1, -3)$, $(+1, -1)$ and $(+3, +1)$ in steps of 20 mm from the focus spot. The rotation of 45° occurs at about 40 mm from the focus.

In order to confirm these experimental results, Fig. 4 shows computer simulations of the experimental conditions. In these simulations, we consider a radially polarized beam of

Optics EXPRESS

$\omega_{01} = 4$ mm that is transmitted through the SLM/*q*-plate system, similar to that used in the experiments. It is generated in an image of 1024 × 1024 pixels that assumes each pixel of $\Delta = 20$ microns (equal to the LCOS-SLM pixel pitch). The beam is then multiplied by the complex transmittance of a lens of focal length f = 100 cm. Fig. 4 clearly confirms the experimental results and show the different behavior around the focus for the three different combinations of charges $(\ell_R, \ell_L) = (-1, -3)$, $(+1, -1)$ and $(+3, +1)$. The size of each image is similar to those of Fig. 3. The simulations match the experimental results very nicely.

5. Experimental system with no moving elements

The difficulty with these experiments is that the center axes of the incident beam, the SPP encoded onto the SLM, the *q*-plate, and the focusing lens (L2) must be very well aligned to obtain such good results. These difficulties are compounded when either the focusing lens or the detector must be moved. To avoid these difficulties we now discuss an alternative, simplified optical setup where the lens L2 is encoded onto the LCoS-SLM. The new setup is shown in Fig. 5(a). The combination of the SPP and the converging lens gives as a result the well-known spiral phase pattern. This pattern can be used to simultaneously impart the SPP to the beam and focusing the beam onto the CCD detector.

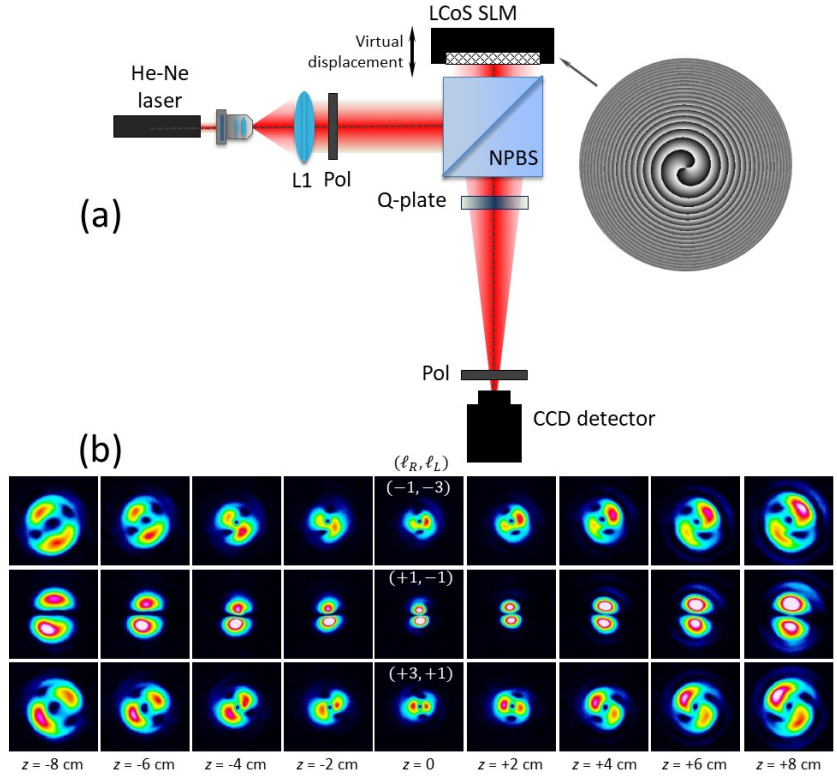

Fig. 5. (a) Scheme of the second proposed optical setup to generate different pure and hybrid vector beams and study Gouy phase effects. A SPP and the lens are encoded on the LCoS-SLM. The CCD camera is kept in a fixed position and the phase mask in the SLM is virtually displaced using a propagation algorithm. (b) Results for the propagation of the radially polarized beams with charges $(\ell_R, \ell_L) = (-1, -3)$, $(+1, -1)$ and $(+3, +1)$. The analyzer is vertically aligned in all cases.

Then, in order to avoid moving the detector, we applied a technique consisting in virtually shifting the axial location of the lens by calculating the corresponding Fresnel diffraction, and

Optics EXPRESS

displaying it onto the SLM [31,32]. Applying a fast Fresnel algorithm [33] it is possible to virtually translate the lens and adjust the position of the focused beam relative to the detector position. Therefore, the same experiments presented in the previous subsection can be performed, but now no element is moving, and all variations are controlled by the SLM. Note, however, two changes with respect to the setup in Fig. 3(a). First, the position of the CCD detector must be changed, since we use the same value (100 cm) for the focal length for the focusing lens, but now it is located on the SLM. Second, and more relevant, now the beam impinging the q-plate is already converging.

Despite the slightly converging beam incident on the q-plate, Fig. 5(b) shows results equivalent to those presented in Fig. 3(b) and simulated in Fig. 4. We first located the beam waist when the regular spiral lens (with focal length of 100 cm) is displayed onto the LCoS-SLM. Then, in order to shift the location of the waist, we applied the fast Fresnel propagation algorithm to the spiral lens, and displayed the new propagated field onto the SLM. Note that both positive and negative propagation distances can be encoded this way. Therefore, we were able to displace the beam waist and experimentally reproduce the results in Fig. 3(b) without having to move the detector. We applied the same propagation distances as measured in Fig. 3(b) and in the simulations. Note the excellent agreement between the results in Fig. 5(b) and Fig. 3(b). This verifies the procedure without moving elements as a very useful way of experimentally investigating these Gouy phase effects.

6. Conclusions

In summary, we have considered a simplified optical system to generate pure and hybrid vector beams, based on the use of a q-plate and an LCoS-SLM. The ability to program different spiral phases on the SLM allows easily changing the topological charges encoded onto the vector beam and compare in a simple manner the polarization patterns and the corresponding intensity patterns when projected onto an analyzer.

This system is then applied to compare the propagation of pure and hybrid vector beams. We have provided a physical insight of the beam polarization transformations upon propagation based on the Gouy phase difference between the RCP and LCP components. This phase difference can be regarded as an optical activity effect that rotates the polarization as the beam propagates. Although the present analysis is only an approximation, it is very useful to obtain a very simple but with still quite good accurate description of the polarization transformation. A more complete description of these kind of transformations can be found for instance in [43].

Experimental results were presented where we capture different axial planes by physically moving the focusing lens. These results were corroborated by numerical simulations. The polarization rotation of the hybrid vector beams approximately follows the classical arctan term $\zeta(z)$ of the Guoy phase. The exact polarization rotation angles depend on the encoded charges of the hybrid vector beam and on the input beam width. Nevertheless, this approximation provides a comprehensive description of the propagation dynamics and polarization transformation of these beams.

Finally, we have shown an alternative and very convenient optical setup, devoid of moving elements, to experimentally evaluate Gouy phase effects. It is based on a codified Fresnel propagation of a spiral lens (combination of a SPP and a focusing lens) encoded onto the SLM. This way we can change the focusing of the output beam from a computer without moving any element.

Funding

Generalitat Valenciana, Conselleria d'Educació, Investigació, Cultura i Esport (PROMETEO-2017-154) and Ministerio de Economía, Industria y Competitividad of Spain and European Union (MIMECO/FEDER funds, grant FIS2015-66328-C3-3-R).

Optics EXPRESS

References

1. Q. Zhan, "Cylindrical vector beams: from mathematical concepts to applications," Adv. Opt. Photonics **1**(1), 1–57 (2009).
2. G. Milione, M. P. J. Lavery, H. Huang, Y. Ren, G. Xie, T. A. Nguyen, E. Karimi, L. Marrucci, D. A. Nolan, R. R. Alfano, and A. E. Willner, "4 × 20 Gbit/s mode division multiplexing over free space using vector modes and a q-plate mode (de)multiplexer," Opt. Lett. **40**(9), 1980–1983 (2015).
3. S. Ramachandran, P. Kristensen, and M. F. Yan, "Generation and propagation of radially polarized beams in optical fibers," Opt. Lett. **34**(16), 2525–2527 (2009).
4. Y. Jin, O. J. Allegre, W. Perrie, K. Abrams, J. Ouyang, E. Fearon, S. P. Edwardson, and G. Dearden, "Dynamic modulation of spatially structured polarization fields for real-time control of ultrafast laser-material interactions," Opt. Express **21**(21), 25333–25343 (2013).
5. I. Moreno, J. A. Davis, I. Ruiz, and D. M. Cottrell, "Decomposition of radially and azimuthally polarized beams using a circular-polarization and vortex-sensing diffraction grating," Opt. Express **18**(7), 7173–7183 (2010).
6. S. C. Tidwell, D. H. Ford, and W. D. Kimura, "Generating radially polarized beams interferometrically," Appl. Opt. **29**(15), 2234–2239 (1990).
7. L. Marrucci, C. Manzo, and D. Paparo, "Optical spin-to-orbital angular momentum conversion in inhomogeneous anisotropic media," Phys. Rev. Lett. **96**(16), 163905 (2006).
8. I. Moreno, M. M. Sánchez-López, K. Badham, J. A. Davis, and D. M. Cottrell, "Generation of integer and fractional vector beams with q-plates encoded onto a spatial light modulator," Opt. Lett. **41**(6), 1305–1308 (2016).
9. C. Maurer, A. Jesacher, S. Fürhapter, S. Bernet, and M. Ritsch-Marte, "Tailoring of arbitrary optical vector beams," New J. Phys. **9**(3), 78 (2007).
10. B. Khajavi and E. J. Galvez, "High-order disclinations in space-variant polarization," J. Opt. **18**(8), 084003 (2016).
11. J. A. Davis, D. M. Cottrell, B. C. Schoonover, J. B. Cushing, J. Albero, and I. Moreno, "Vortex sensing analysis of radially and pseudo-radially polarized beams," Opt. Eng. **52**(5), 50502 (2013).
12. A. M. Beckley, T. G. Brown, and M. A. Alonso, "Full Poincaré beams," Opt. Express **18**(10), 10777–10785 (2010).
13. A. Niv, G. Biener, V. Kleiner, and E. Hasman, "Manipulation of the Pancharatnam phase in vectorial vortices," Opt. Express **14**(10), 4208–4220 (2006).
14. X. Ling, X. Yi, Z. Dai, Y. Wang, and L. Chen, "Characterization and manipulation of full Poincaré beams on the hybrid Poincaré sphere," J. Soc. Opt. Am. B **33**(11), 2172–2176 (2016).
15. Z. Liu, Y. Liu, Y. Ke, Y. Liu, W. Shu, H. Luo, and S. Wen, "Generation of arbitrary vector vortex beams on hybrid-order Poincaré sphere," Photon. Res. **5**(1), 15–21 (2017).
16. J. A. Davis, D. E. McNamara, D. M. Cottrell, and T. Sonehara, "Two-dimensional polarization encoding with a phase-only liquid-crystal spatial light modulator," Appl. Opt. **39**(10), 1549–1554 (2000).
17. Y. He, H. Ye, J. Liu, Z. Xie, X. Zhang, Y. Xiang, S. Chen, Y. Li, and D. Fan, "Order-controllable cylindrical vector vortex beam generation by using spatial light modulator and cascaded metasurfaces," IEEE Photonics J. **9**(5), 1 (2017).
18. M. M. Sánchez-López, I. Abella, D. Puerto-García, J. A. Davis, and I. Moreno, "Spectral performance of a zero-order liquid-crystal polymer commercial *q*-plate for the generation of vector beams at different wavelengths," Opt. Laser Technol. **106**, 168–176 (2018).
19. E. J. Galvez, S. Khadka, W. H. Schubert, and S. Nomoto, "Poincaré-beam patterns produced by nonseparable superpositions of Laguerre-Gauss and polarization modes of light," Appl. Opt. **51**(15), 2925–2934 (2012).
20. C.-H. Yang, Y.-D. Chen, S.-T. Wu, and A. Y.-G. Fuh, "Independent manipulation of topological charges and polarization patterns of optical vortices," Sci. Rep. **6**(1), 31546 (2016).
21. G. M. Philip, V. Kumar, G. Milione, and N. K. Viswanathan, "Manifestation of the Gouy phase in vector-vortex beams," Opt. Lett. **37**(13), 2667–2669 (2012).
22. H. Wang, G. Rui, and Q. Zhan, "Dynamic propagation of optical vortices embedded in full Poincaré beams with rotationally polarization symmetry," Opt. Commun. **351**, 15–25 (2015).
23. K. J. Kaltenecker, J. C. König-Otto, M. Mittendorff, S. Winnerl, H. Schneider, M. Helm, H. Helm, M. Walther, and B. M. Fischer, "Gouy phase shift of a tightly focused, radially polarized beam," Optica **3**(1), 35–41 (2016).
24. Y. Zhang, X. Guo, L. Han, P. Li, S. Liu, H. Cheng, and J. Zhao, "Gouy phase induced polarization transition of focused vector vortex beams," Opt. Express **25**(21), 25725–25733 (2017).
25. P. Pääkkönen, J. Lautanen, M. Honkanen, M. Kuittinen, J. Turunen, S. N. Khonina, V. V. Kotlyar, V. A. Soifer, and A. Friberg, "Rotating optical fields," J. Mod. Opt. **45**(11), 2355–2369 (1998).
26. J. A. Davis and J. B. Bentley, "Azimuthal prism effect with partially blocked vortex-producing lenses," Opt. Lett. **30**(23), 3204–3206 (2005).
27. P. Vaity and R. P. Singh, "Self-healing property of optical ring lattice," Opt. Lett. **36**(15), 2994–2996 (2011).
28. H. X. Cui, X. L. Wang, B. Gu, Y. N. Li, J. Chen, and H. T. Wang, "Angular diffraction of an optical vortex induced by the Gouy phase," J. Opt. **14**(5), 055707 (2012).
29. X.-L. Wang, K. Lou, J. Chen, B. Gu, Y. Li, and H.-T. Wang, "Unveiling locally linearly polarized vector fields with broken axial symmetry," Phys. Rev. A **83**(6), 063813 (2011).

Optics EXPRESS

30. P. Srinivas, C. Perumangatt, N. Lal, R. P. Singh, and B. Srinivasan, "Investigation of propagation dynamics of truncated vector vortex beams," Opt. Lett. **43**(11), 2579–2582 (2018).
31. J. A. Davis, I. Moreno, D. M. Cottrell, C. A. Berg, C. L. Freeman, A. Carmona, and W. Debenham, "Experimental implementation of a virtual optical beam propagator system based on a Fresnel diffraction algorithm," Opt. Eng. **54**(10), 103101 (2015).
32. I. Moreno, J. A. Davis, T. Womble-Dahl, and D. M. Cottrell, "Azimuthal multiple-beam interference effects with combinations of vortex beams," Opt. Lett. **40**(10), 2341–2344 (2015).
33. J. A. Davis and D. M. Cottrell, "Ray matrix analysis of the fast Fresnel transform with applications towards liquid crystal displays," Appl. Opt. **51**(5), 644–650 (2012).
34. B. E. A. Saleh and M. C. Teich, *Fundamentals of Photonics*, 2nd edition, (John Wiley and Sons Inc. 2007).
35. S. Ngcobo, K. Aït-Ameur, N. Passilly, A. Hasnaoui, and A. Forbes, "Exciting higher-order radial Laguerre-Gaussian modes in a diode-pumped solid-state laser resonator," Appl. Opt. **52**(10), 2093–2101 (2013).
36. M. J. Padgett and L. Allen, "The Poynting vector in Laguerre-Gaussian laser modes," Opt. Commun. **121**(1-3), 36–40 (1995).
37. S. G. Reddy, C. Permangatt, S. Prabhakar, A. Anwar, J. Banerji, and R. P. Singh, "Divergence of optical vortex beams," Appl. Opt. **54**(22), 6690–6693 (2015).
38. M. J. Padgett, F. M. Miatto, M. P. J. Lavery, A. Zeilinger, and R. W. Boyd, "Divergence of an orbital-angular-momentum-carrying beam upon propagation," New J. Phys. **17**(2), 023011 (2015).
39. E. Hetch, *Optics*, 5th edition, Pearson Education Limited (2017).
40. J. A. Davis, B. M. L. Pascoguin, I. Moreno, and A. Nava-Vega, "Circular-polarization-splitting common-path interferometer based on a zero-twist liquid-crystal display," Opt. Lett. **34**(9), 1486–1488 (2009).
41. A. Yariv, *Quantum Electronics*, 3rd edition, (John Wiley & Sons, 1989).
42. A. P. Porfirev, A. V. Ustinov, and S. N. Khonina, "Polarization conversion when focusing cylindrically polarized vortex beams," Sci. Rep. **6**(1), 6 (2016).
43. C. N. Alexeyev, Yu. A. Egorov, and A. V. Volyar, "Mutual transformations of fractional-order and integer-order optical vortices," Phys. Rev. A **96**(6), 63807 (2017).